

Quantum device simulation with a generalized tunneling formula

Gerhard Klimeck,^{a)} Roger Lake,^{a)} R. Chris Bowen, William R. Frensley, and Ted S. Moise^{a)}

Eric Jonsson School of Engineering, University of Texas at Dallas, Richardson, Texas 75083-0688

(Received 9 June 1995; accepted for publication 16 August 1995)

We present device simulations based on a generalized tunneling theory. The theory is compatible with standard coherent tunneling approaches and significantly increases the variety of devices that can be simulated. Quasi-bound and continuum states in the leads are treated on the same footing. Quantum charge self-consistency is included in the leads and the central device region. We compare the simulated I - V characteristics with the experimental I - V characteristics for two complex quantum device structures and find good agreement. © 1995 American Institute of Physics.

Many resonant tunneling based semiconductor devices have complicated structure in the emitter or collector regions due to electrostatic band bending or heteroepitaxial confinement^{1,2} (see Figs. 1 and 2). For such devices, the usual coherent tunneling approaches compared by Landheer and Aers³ are inadequate. Neither the approach of Cahay *et al.*⁴ nor the approach of Onishi *et al.*⁵ can model electron injection from quasi-bound states in the emitter. The treatments of scattering described by Lake and Datta,⁶ Roblin and Liou,⁷ or Chevoir and Vinter⁸ are insufficient either in principle, e.g., the first-order approach of Chevoir and Vinter,⁸ or in practice due to the computational and memory requirements of modeling a long structure with extreme thermalization of the carriers.^{6,7} There have been a number of efforts to model injection from emitter quasi-bound states,^{9,10} but the resulting theory is *ad hoc* and treats the emitter quasi-bound

states in a different manner from the emitter continuum states. The generalized tunneling formula described by Lake *et al.*¹¹ allows a general, unified treatment of emitter quasi-bound states and emitter continuum states. It allows one to partition, when appropriate, a long structure into two large reservoirs with spatially varying potentials and a short “device” (see Figs. 1 and 2). The theory treats thermalization and scattering induced broadening in the reservoirs with no more effort than the standard coherent tunneling approaches.³ We present simulations based on the theory. We find the device simulator to be capable of modeling a wider range of devices than those based on the standard approaches,³ and we obtain good agreement between the experimental data and the numerical results.

We present a brief overview of the theory used to obtain the generalized tunneling formula. The Hamiltonian is written as the sum of three terms: $H_o = H_o^D + H_o^L + H_o^R$ which represent the Hamiltonian of the device, the left reservoir, and the right reservoir, respectively. The Hamiltonian matrix is written in terms of the tight-binding basis $\langle \mathbf{r} | \mathbf{k}, n \rangle = e^{i\mathbf{k} \cdot \mathbf{r}} \phi_n(z) / \sqrt{A}$ where \mathbf{k} is the transverse wavevector, A is the cross-sectional area, and $\phi_n(z)$ is a localized

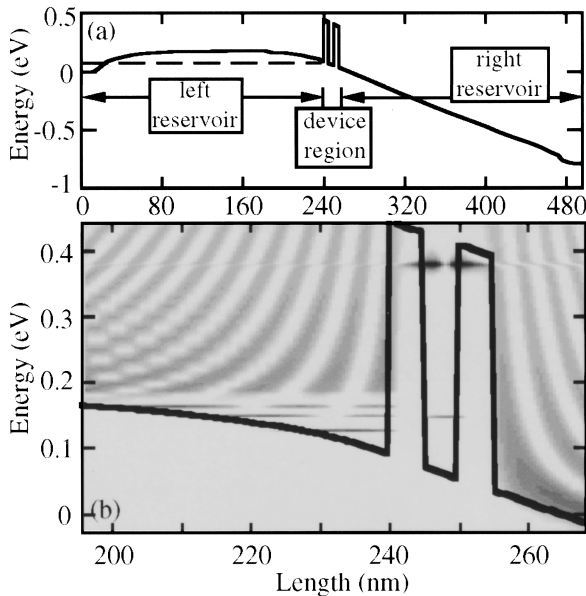


FIG. 1. (a) Conduction band profile for a $\text{Al}_{0.4}\text{Ga}_{0.6}\text{As}/\text{GaAs}$ resonant tunneling diode (RTD) from Ref. 1. Dashed line in the emitter indicates the Fermi level. The structure is divided into 3 regions: left and right reservoir and a central “device” region. (b) Spectral function of the resonant tunneling diode close to the central device region plotted versus longitudinal energy and position. Magnitude increases with shading. Emitter quasi-bound states in the triangular potential well are evident.

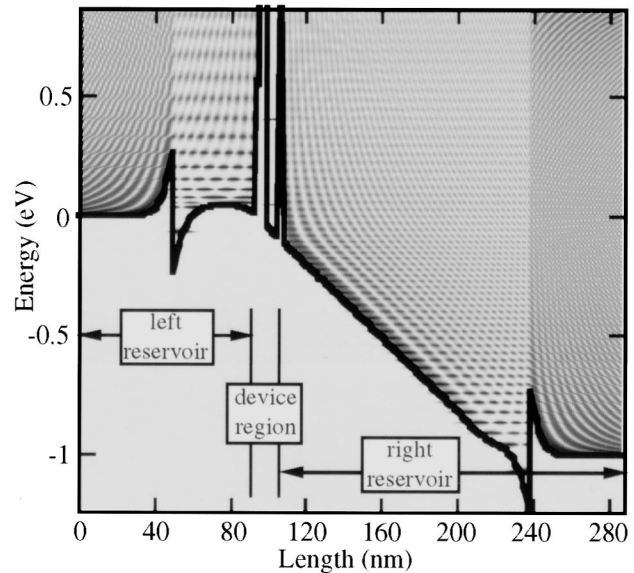


FIG. 2. Conduction band profile and spectral function plotted versus longitudinal energy and position of an $\text{InGaAs}/\text{AlAs}$ Opto-RTD (ORTD) similar to the one in Ref. 2. Magnitude of spectral function increases with shading. Multiple states in the emitter potential well are evident.

^{a)}Corporate R&D, Texas Instruments Incorporated, Dallas, TX 75265.

(Wannier) function localized around site “ n ”. The matrix elements of H_o are $\langle \mathbf{k}, i | H_o | \mathbf{k}, j \rangle = \epsilon_{\mathbf{k}} \delta_{i,j} - t_{i,j} \delta_{i,j \pm 1}$. The site energies and hopping elements can be related to the discretized effective mass Hamiltonian, $H_o = -\hbar^2/2 d/dz 1/m^*(z) d/dz + V_k(z)$ in the usual way.^{11,12}

For a device consisting of sites $1, \dots, N$, the effect of the left and right reservoirs, and the coupling to the reservoirs, $t_{0,1}$ and $t_{N,N+1}$, are treated *exactly* using Dyson’s equation to obtain the boundary self energies:^{11,13}

$$\Sigma_{1,1}^{RB} = g_{0,0}^R |t_{0,1}|^2 \quad \text{and} \quad \Sigma_{N,N}^{RB} = g_{N+1,N+1}^R |t_{N,N+1}|^2, \quad (1)$$

$$\Gamma_{1,1}^B = a_{0,0} |t_{0,1}|^2 \quad \text{and} \quad \Gamma_{N,N}^B = a_{N+1,N+1} |t_{N,N+1}|^2, \quad (2)$$

where g^R is the Green function of the reservoir unconnected to the device ($t_{0,1} = t_{N,N+1} = 0$) and a is the corresponding spectral function, $a = -2\text{Im}g^R$. The boundary self-energies Σ^{RB} and Γ^B are valid even if the reservoirs have spatially varying potentials. The self-energies in Eqs. (1)–(2) are zero for sites $\{i, j\} \neq \{1, 1\}$ or $\{N, N\}$.

The equation of motion for G^R in the device becomes (in matrix notation) $(E - H_o^D - \Sigma^{RB})G^R = 1$. An explicit representation of the retarded Green function for a device of three sites is

$$[G^R] = \begin{bmatrix} E - \epsilon_{\mathbf{k},1} - \Sigma_{1,1}^{RB} & t_{1,2} & 0 \\ t_{2,1} & E - \epsilon_{\mathbf{k},2} & t_{2,3} \\ 0 & t_{3,2} & E - \epsilon_{\mathbf{k},3} - \Sigma_{3,3}^{RB} \end{bmatrix}^{-1}. \quad (3)$$

To calculate the self energies $\Sigma_{1,1}^{RB}$ and $\Gamma_{1,1}^B$, we need $g_{0,0}^R$. For a left reservoir in which the semi-infinite uniform potential region begins at site -2 , $g_{0,0}^R$ is found from

$$g_{0,0}^R = \begin{bmatrix} -t_L e^{-i\gamma - 2\Delta} & t_{-2,-1} & 0 \\ t_{-1,-2} & E - \epsilon_{\mathbf{k},-1} & t_{-1,0} \\ 0 & t_{0,-1} & E - \epsilon_{\mathbf{k},0} \end{bmatrix}_{0,0}^{-1}, \quad (4)$$

where γ is the longitudinal propagation factor of the left contact and Δ is the site spacing.^{11,12} The desired elements of G^R and g^R needed for the calculation of the self-energies, the electron density, and the current can be obtained from Eqs. (3) and (4) by any matrix inversion technique, but we find the recursive Green function algorithm¹⁴ to be the most efficient.

True bound states may be present in the spectrum of $g_{0,0}^R$ since $t_{0,1} = 0$. To avoid this, an energy dependent optical potential, $-i\sigma$, is added to the site energies, $\epsilon_{\mathbf{k},i}$, in the reservoirs. The optical potential is set to zero for energies below the conduction band edge to avoid unrealistic band tails. Any spatial or energy dependence can be used, and we plan to explore more realistic models. Physically, the optical potential represents the scattering induced broadening; if an emitter quasi-bound state is to act as a reservoir, it must be coupled to the continuum of states to the left through inelastic channels. The optical potential is an approximation for the imaginary part of the retarded self energy due to scattering in the reservoirs. The values of σ used for the simulation of the devices shown in Figs. 1 and 2 were empirically taken to be 6.6 meV and 15 meV, respectively. These values are similar

to the ones used by Chen *et al.*¹⁰ who discuss the physical validity of these values, and, like Chen *et al.*, we also find that a good quantitative fit is impossible if the broadening is not taken into account. We also find that the effective broadening introduced by proper integration over the transverse momentum¹⁵ is not sufficient to obtain good agreement with the experimental data when emitter quasi-bound states are present. The optical potential is non-zero only in the reservoirs (see Fig. 2) and zero in the device. Therefore, in the device, where current is calculated, current is conserved.

We calculate the electrostatic potential profile both in the Thomas–Fermi approximation¹⁶ and in the Hartree approximation by solving Poisson’s equation self-consistently with the quantum charge. For the self-consistent calculation, the electron density is calculated from

$$N_i = \frac{1}{A\Delta} \sum_{\mathbf{k}} \int \frac{dE}{2\pi} n_i(\mathbf{k}, E).$$

In the reservoirs, n_i is calculated from the equilibrium relation, $n_i = f_{L(R)}(-2)\text{Im}G_{i,i}^R$ where G^R is the exact Green function of the *connected* reservoir, and in the device, n_i is calculated from $n_i = f_L \Gamma_{1,1}^B |G_{i,1}^R|^2 + f_R \Gamma_{N,N}^B |G_{i,N}^R|^2$ where $f_{L(R)}$ is the Fermifactor of the left (right) contact.

With a converged solution of N_i and the electrostatic potential, the current is then calculated. The expression for the current can be cast into the form of the usual tunneling formula with a generalized Fisher–Lee form for the transmission coefficient,¹¹

$$J_{1/2} = \frac{2e}{\hbar A} \sum_{\mathbf{k}} \int \frac{dE}{2\pi} \Gamma_{1,1}^B \Gamma_{N,N}^B |G_{1,N}^R|^2 (f_L - f_R). \quad (5)$$

In Eq. (5), the Γ^B ’s are no longer simply factors of velocity, but take into account the effect of spatially varying potentials.

The Fermi factors of the contacts appear for the first time in the equations for the electron density and the current. These expressions are valid provided that the reservoir regions in Figs. 1 and 2 are well equilibrated with the n^+ contacts at the left and right of the structures.

We model two different devices at room temperature (300 K). The first is an experimental GaAs/Al_{0.4}Ga_{0.6}As resonant tunneling diode (RTD) corresponding to Fig. 2(d) of Ref. 1. Figure 1 shows the conduction band profile and corresponding spectral function, $A(E, \mathbf{k}=0) = -2\text{Im}G^R(E, \mathbf{k}=0)$, calculated around the central quantum region. Several closely spaced emitter quasi-bound states forming an electron accumulation layer are evident. Figure 3 compares our simulation results to the experimental data.¹ Figure 1(b) shows the quantum well resonance aligned with the second emitter quasi-bound state at a bias of about 1 V. This alignment results in the step-like feature of the I – V plot. Our simulations confirm the arguments presented in Ref. 1 that the step feature results from the alignment of the second emitter quasi-bound state with the resonant state in the well and that the main peak results from the alignment of the lowest emitter quasi-bound state with the resonant state in the well.

The Thomas–Fermi approximation gives rough agreement with the experimental data with a computation time of

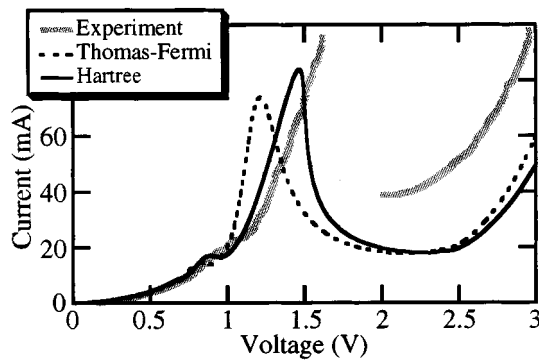


FIG. 3. Experimental and simulated I - V characteristics for the RTD corresponding to Fig. 1. The thick gray line is the experimental data that we have digitized from Ref. 1. The short dashed line results from a Thomas-Fermi calculation of the electrostatic potential. The solid results from a Hartree self-consistent calculation of the electrostatic potential throughout the whole structure.

about 0.75 sec per bias point on an HP 735 workstation. Hartree self-consistency increases the accuracy at a cost of 30 times the cpu time. The peak current remains about 8% lower than the experimental result. Preliminary calculations indicate that this deviation results from band-structure effects which we will address in the future.

The second device we model is an InP lattice matched InGaAs/InAlAs opto-RTD (ORTD) with strained AlAs barriers similar to the one described in Ref. 2. The structure consists of a 5.5 nm InGaAs well and 2.6 nm AlAs barriers. The emitter barrier has an additional 2.3 nm InAlAs pre-barrier. The emitter consists of a 40 nm InGaAs well doped at 10^{18} cm^{-3} , preceded by a 200 nm InAlAs layer doped at $5 \times 10^{18} \text{ cm}^{-3}$ graded to a 500 nm InGaAs layer doped at $5 \times 10^{18} \text{ cm}^{-3}$ and the InP substrate. The collector consists of a 100 nm undoped InGaAs and a 30 nm 10^{18} cm^{-3} doped InGaAs spacer, a 200 nm InAlAs window and a 40 nm InGaAs cap both doped at $5 \times 10^{18} \text{ cm}^{-3}$. Fig. 2 shows the conduction band profile and corresponding spectral function for the ORTD truncated in the emitter and collector InAlAs regions. Figure 4 compares the simulation results using Thomas-Fermi and Hartree self-consistent electrostatic calculations against the experimental data. While the Thomas-Fermi simulation follows the general trend of the experimental data, the Hartree self-consistent calculation provides far better quantitative comparison. The features in the turn-on of the peak current result from the quantized states in the emitter aligning with the state in the well.

In summary, we have presented a device simulator which implements a generalized tunneling theory based on a novel treatment of the contacts. The theory takes the form of stan-

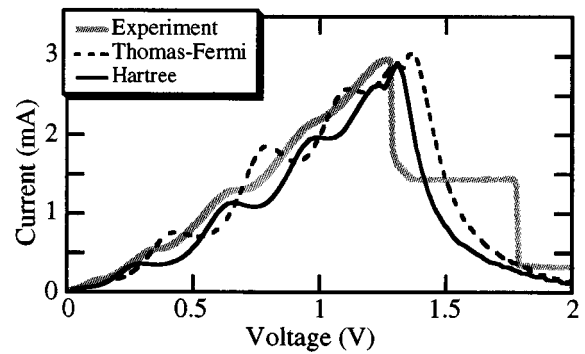


FIG. 4. Experimental and simulated I - V characteristics based on new boundary conditions for the ORTD corresponding to Fig. 2. The gray line is the experimental data. The dashed line is the simulation resulting from a Thomas-Fermi calculation of the electrostatic potential. The thin solid line is the simulation resulting from a Hartree self-consistent calculation of the electrostatic potential throughout the whole structure.

dard coherent tunneling approaches, Eq. (5). The novel treatment of the contacts, Eqs. (1)–(4), combined with Hartree self consistency is sufficient to obtain reasonable quantitative agreement with a number of complex quantum devices which are modeled poorly by the standard approaches.³

We acknowledge the benefit of many conversations with D. Jovanovic.

- ¹J. S. Wu *et al.*, *Solid State Electron.* **34**, 403 (1991).
- ²T. S. Moise, Y. Kao, L. D. Garrett, and J. C. Campbell, *Appl. Phys. Lett.* **66**, 1104 (1995).
- ³D. Landheer and G. C. Aers, *Superlattices Microstruct.* **7**, 17 (1990).
- ⁴M. Cahay, M. J. McLennan, S. Datta, and M. S. Lundstrom, *Appl. Phys. Lett.* **50**, 612 (1987).
- ⁵H. Ohnishi, T. Inata, S. Muto, N. Yokoyama, and A. Shibatomi, *Appl. Phys. Lett.* **49**, 1248 (1986).
- ⁶R. Lake and S. Datta, *Phys. Rev. B* **45**, 6670 (1992).
- ⁷P. Roblin and W. Liou, *Phys. Rev. B* **46**, 2416 (1993).
- ⁸F. Chevoir and B. Vinter, *Phys. Rev. B* **47**, 7260 (1993).
- ⁹T. Fiig and A. Jauho, *Surf. Sci.* **267**, 392 (1992).
- ¹⁰J. Chen, G. Chen, C. H. Yang, and R. A. Wilson, *J. Appl. Phys.* **70**, 3131 (1991); J. Chen, C. H. Yang, and R. A. Wilson, *ibid.* **71**, 1537 (1992).
- ¹¹R. Lake, in *Quantum Device Modeling with Non-Equilibrium Green Functions*, edited by D. K. Ferry, H. L. Grubin, and C. Jacoboni (Plenum Press, New York, 1995), p. 521–524; R. Lake, G. Klimeck, and R. C. Bowen, *Modeling of Wide Cross-Sectional Area, 1-D, Steady-State, High-bias Quantum Devices: Theory* (unpublished).
- ¹²W. R. Frensley, in *Heterostructures and Quantum Devices*, edited by N. Einspruch and W. R. Frensley (Academic Press, New York, 1994), pp. 273–303.
- ¹³S. Hershfield, J. H. Davies, and J. W. Wilkins, *Phys. Rev. B* **46**, 7046 (1992); Y. Meir and N. S. Wingreen, **68**, 2512 (1992).
- ¹⁴J. A. Støeneng and E. H. Hauge, *Phys. Rev. B* **44**, 13582 (1991).
- ¹⁵T. B. Boykin, R. E. Carnahan, and K. P. Martin, *Phys. Rev. B* **51**, 2273 (1995).
- ¹⁶J. H. Luscombe, *Nanotechnology* **4**, 1 (1993).